Linear and radial flow modelling of a waterflooded, stratified, non-communicating reservoir developed with downhole, flow control completions

Journal Pre-proof

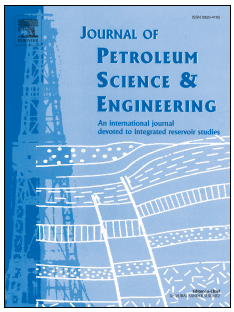

Linear and radial flow modelling of a waterflooded, stratified, non-communicating reservoir developed with downhole, flow control completions

Bona Prakasa, Khafiz Muradov, David Davies

PII: S0920-4105(19)30761-2

DOI: https://doi.org/10.1016/j.petrol.2019.106340

Reference: PETROL 106340

To appear in: *Journal of Petroleum Science and Engineering*

Received Date: 26 May 2019

Revised Date: 1 August 2019

Accepted Date: 3 August 2019

Please cite this article as: Prakasa, B., Muradov, K., Davies, D., Linear and radial flow modelling of a waterflooded, stratified, non-communicating reservoir developed with downhole, flow control completions, *Journal of Petroleum Science and Engineering* (2019), doi: https://doi.org/10.1016/j.petrol.2019.106340.

Linear and radial flow modelling of a waterflooded, stratified, non-communicating reservoir developed with downhole, flow control completions

Summary

Forecasts of the performance of waterflooded oil-field have been prepared for many years using fractional flow models, such as those by (Buckley-Leverett, 1942) (BL), (Welge, 1952) and (Dykstra-Parsons, 1950) (DP), to estimate the vertical sweep efficiency between wells. These methods, and their later modifications, formed the theoretical basis for designing a water-flooded oil-field. Advanced Well Completions (AWC) incorporating downhole flow control device (FCD) technology have become a proven method for modifying a production well's inflow profile, delaying water breakthrough, improving sweep efficiency and enhancing recovery.

This manuscript extends the fractional flow model describing the performance of a waterflooded, stratified-reservoir with an AWC installed in the production well. The piston-like behaviour of the water-front described by previous, semi-analytical models is extended here to the linear and radial flow modelling of more realistic displacement profiles.

This paper describes the theoretical basis and application workflow along with several case studies illustrating their performance and value. The accuracy of the new, semi-analytical models are verified by comparison against the results from a numerical reservoir simulator. Model limitations and possible future extension are also discussed.

The workflow can be implemented as either a production forecast or a diagnostic tool for an AWC well in a waterflooded oil-field. It provides one missing link between today's AWC design workflows and the long-term value evaluation of a specific AWC design when a commercial numerical simulation software is either not available or too time consuming.

1. Introduction

Researchers have developed simplified performance and analysis methods based on (semi-) analytical solutions and type curves for a range of well control situations, well patterns and geological environments in a waterflooded oil-field. These simplified analysis methods are still routinely used today, despite the wide availability of numerical reservoir simulators.

The oil recovery factor is the product of the oil efficiency displacement at the pore level and the volumetric sweep efficiency. The latter, a product of the areal and vertical sweep efficiencies, is a function of the flood pattern, geological discontinuities, mobility ratio, etc. The vertical sweep efficiency between an injection and production well pair depends on the reservoir heterogeneity with more permeable layers being flooded faster.

(Buckley and Leverett, 1942) provided the first description of two-phase, immiscible displacement of oil by water in a linear (1D) pore system. Their BL model described the velocity water propagation through the linear system. (Welge, 1952)'s W model calculates the average saturation behind the water front, establishing a relationship between the average water saturation as a function of either the cumulative volume of water injected or the total injection time. They are recognised as proven methods for forecasting oil recovery with conventional wells, but are not applicable to production wells completed with DFC, a technology designed to mitigate unevenly propagating waterflood fronts in heterogeneous reservoirs.

The areal sweep and oil displacement efficiencies has been widely studied, e.g. the (Dyes et al., 1954) mathematical model or core flooding experiments. This paper presents a new method to predict and analyse the vertical sweep efficiency of an oil field developed with AWC production wells. Analytical solutions for the vertical sweep efficiency of a heterogeneous reservoir refer to either non-communicating or to perfectly communicating layers with instantaneous pressure equilibrium.

The (Dykstra and Parsons, 1950) (DP) model analysed the case of non-communicating layers case with arbitrary properties. Their analytical solutions estimate the recovery efficiency and the fractional flow curve of each layer as a function of the volume of injected water. They also derived general formulae and type curves for a reservoir with a vertical, log-normal, permeability distribution. (Muscat, 1950) derived expressions for other permeability distributions while (Johnson, 1956) extended the solutions to cases where the water-oil viscosity ratio is no longer one. (Synder and Ramey, 1967) used elements of BL theory to add non-piston-like displacement, note that non-piston like displacement occurs when the mobility ratio is significantly higher or lower than one. (Osman and Tiab, 1981) extended the model to composite layers with lateral permeability variation while (Reznik et al., 1984) and (El-Khatib, 1985) translated the results into the time domain.

(Warren, 1964) and (Goddin et al., 1966) considered the effect of crossflow between layers. Solutions for waterflood analysis in reservoirs with communicating layers were presented by (Hiatt, 1958) and extended to reservoirs with layers of variable properties (El-Khatib, 1985), log-normally distributed vertical permeability (El-Khatib, 1999), gravity driven cross-flow (El-Khatib, 2003) and even inclined reservoirs (El-Khatib, 2010). Finally, (Muradov, et al., 2018) extended the DP model to AWC wells for stratified-reservoir waterfloods with piston-like oil-water displacement behaviour typical of fluids with a mobility ratio close to unity. Their solution included the non-linear, pressure versus flow rate performance of FCDs.

Waterflood performance with radial flow was analysed by (Muscat, 1950) while (Deppe, 1961) predicted the changing injection rates in radial flow for cases with unequal fluid mobility and irregular well patterns. (Rossen, et al., 2008) extend fractional-flow methods for two-phase flow to non-Newtonian fluids in one-dimensional cylindrical flow, where rheology changes with radial position, r, thus allow the fractional-flow curve as a function of radial position. Wu, et al., 2010, presented analytical solutions for non-Darcy flow linear and radial composite reservoir based on Forchheimer and Barree-Conway solution. Mijic, A., and T. C. LaForce (2012) presented the extension of the Buckley-Leverett analytical solution in radial flow when the injected gas phase flow is governed by the two-phase extension to the Forchheimer equation and the fractional flow function depends both on the saturation and radial distance from the well. Evaluation of a peripheral waterflood was presented by (Ling, 2016) using a fractional flow approach to solve for radial flow. This paper shows how fractional flow analysis can be applied to predicting the performance of an AWC well.

The (Halliburton, 2017), steady-state wellbore simulator is the most frequently used tool to predict the performance of an AWC well. This workflow provides a good estimate of the AWC well's performance for the well and near-wellbore reservoir parameters at a specific time. However, (Livescu et al., 2010) recognised that the preferred AWC design for early-time production parameters may no longer be optimum once the long-term well's performance (cumulative oil and water, sweep efficiency, etc.) are considered.

This paper develops a simple, practical workflow to evaluate the long-term performance of an AWC well without the need for numerical, reservoir simulation software. The novel aspects of this work are the extension of the:

1. Welge method with a more accurate relative permeability value of the formation behind a displacement he front at a given average water saturation.
2. Analytical, Buckley-Leverett fractional-flow analysis workflow of non-piston like displacement of reservoir fluids flowing towards an AWC well. Solutions for both linear and radial flow are provided.
3. Model to quantify the change in the FCD's restriction as a function of the water cut.

2. Review of fractional flow analysis and the extended P method to include AWCs

AWC wells are employed when producing from zones of differing reservoir quality, such as heterogeneous reservoirs, differentially depleted layers, compartmentalized

reservoirs, multiple-reservoir developments, unfavourably saturated (e.g. oil-rim) reservoirs, etc. Passive FCD also reduce a long completion's "heel-to-toe effect"(Birchenko et al., 2010a,b). AWC can be installed in a horizontal, deviated or multi-lateral well. An AWC well has between one and hundreds of FCDs installed in the production tubing opposite the production interval.

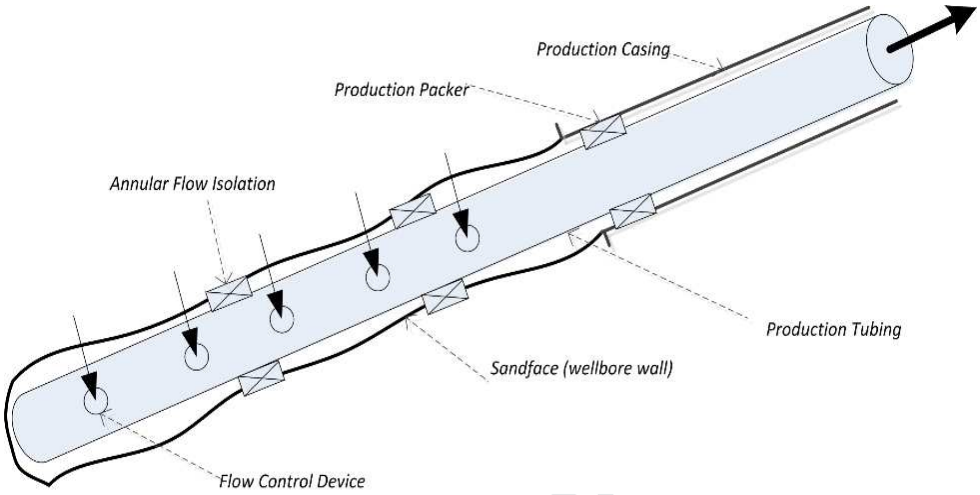

Figure 1: Schematic view of a well with an AWC.

Figure 1 is a schematic view of an open-hole AWC installed with three packers providing annular flow isolation. Optimum AWC design is a complex mathematical problem requiring specification of the FCD type, restriction level and the number of devices. The performance of these FCDs can be represented with the help of a simple empirical constant, called the segment's FCD strength (a), and the segment flow rate (Q).

$$\Delta P_{ICD} = aQ^2 \qquad (1)$$

where *a,* the 'strength' parameter relates the extra pressure drop, ΔP, added by the fluid flow rate, *Q*. (Al-Khelaiwi, 2013) provides formulae to quantify the 'strength' parameter.

The pressure drop across the FCD's restriction is a non-linear function of the fluid flow rate (equation 1), unlike the linear dependence of the reservoir pressure drop. A greater pressure drop occurs across those FCDs with a higher inflow rate. The result is a more uniform inflow profile along the length of the completion compared with that expected from a conventional (open-hole or perforated) completion. FCDs may be Passive *(a fixed restriction)*, Active *(a surface controlled restriction)* or autonomous *(the restriction increases when producing an unwanted fluid).* (Eltaher et al. 2014, Al- Khelaiwi et al. 2008) a good overview of the various types of FCD technology, their evolution and their applications.

i. *Passive* FCD designs are all essentially a fixed restriction that obeys equation 1.
ii. *Active* FCDs typically have between 2 and 10 positions, each of which has a different 'strength' value described by equation 1 { see (Haghighat Sefat et al. 2016}.
iii. *Autonomous* FCDs restrict the flow (Eltaher et al. 2014) in the presence of an unwanted fluid phase (free gas and/or water). The 'strength' parameter is now a function of the type of (single-phase) fluid and the phase-cut (Eltaher et al., 2018; Muradov et al., 2018).

The industry's standard, FCD snapshot design uses a stand-alone wellbore simulator coupled to near-wellbore reservoir simulation {e.g. (Halliburton, 2017)}. The wellbore model optimises the "added-value" by altering the AWC performance specifications to reduce the flow imbalance between zones while avoiding too great a restriction to the inflow performance. This fast, simplified approach improves the initial (oil) production and is assumed to increase the oil long recovery. This assumption is normally not rigorously tested by reservoir simulation.

Alternative, snapshot models exist. (Birchenko et al., 2010) developed analytical and semi-analytical methods to reduce the "heel-toe effect" in homogeneous and heterogeneous

(Birchenko et al., 2011) reservoirs. (Al-Khelaiwi 2013) proposed numerical workflow based on a wellbore model as well as an inflow-outflow balance method. (Prakasa et al, 2015, Prakasa et al, 2019) employed a type-curve method for FCD completion design.

Snapshot methods lack the ability to predict the AWC's long-term impact on the oil recovery efficiency of the waterflood. Traditionally, prediction of the long-term, reservoir performance requires use of a complex, time intensive, coupled wellbore-reservoir simulator. This paper offers an alternative to this problem.

2.1. Fractional flow analysis (linear immiscible displacement)

The BL model describes two-phase, immiscible displacement in a linear system. Equation 2, the fractional flow equation, leads to equation 3 which calculates the location (x) of a given water saturation (S_w), with following assumptions: capillary pressure effects can be neglected, no dip, thus gravity forces can be neglected, homogeneous and isotropic porous medium.

$$fw = \frac{1+\frac{Akk_{ro}}{q_t\mu_o}\left(\frac{\partial P_c}{\partial x}\right)}{1+\frac{k_{ro}\,\mu_w}{k_{rw}\,\mu_o}} \tag{2}$$

$$(x)_{Sw} = \frac{tq_t}{A\Phi}\frac{\partial f_w}{\partial S_w}\Big|_{S_w} \tag{3}$$

fw is fractional flow or the ratio of the flow of water at any point, A is cross-section area, k is permeability, k_{ro} and k_{rw} is relative permeability of oil and water respectively, q_t is total rate, μ_o and μ_w is viscosity of oil and water respectively, P_c is capillary pressure, t is time, Φ is porosity, S_w is water saturation.

(Welge, 1952) evaluated the average saturation behind the water front by drawing a tangent to the fw curve originating at the initial water saturation (Sw_i) (Figure 2). Point A, the intersection, is Sw at the flood front and the reciprocal of the slope is the water front's velocity. The average saturations behind this front is found by extrapolating the tangent $fw = 1$.

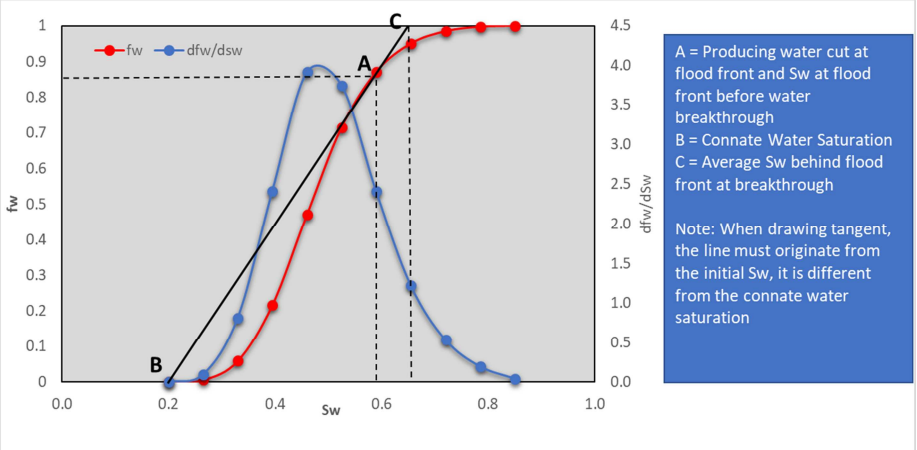

Figure 2: An example of fractional flow curves analysis

(Welge, 1952) determined the average water saturation at breakthrough $(\overline{Sw_{bt}})$, point B in figure 2, by integrating the water saturation over the distance from the point of injection to value of the saturation at the flood front. The calculation continues post-breakthrough (equation 4) with the tangent line to $f_w = 1$ being drawn to find the average water saturation The calculation stops once the layer is fully saturated with water, i.e. when $(S_w = 1 - So_r)$.

$$Sw_{avg} = \overline{S_w} = S_{wf} + \left(\frac{1-fw}{\frac{\delta f_w}{\delta S_w}}\right) \tag{4}$$

2.2. Fractional flow analysis (radial immiscible displacement)

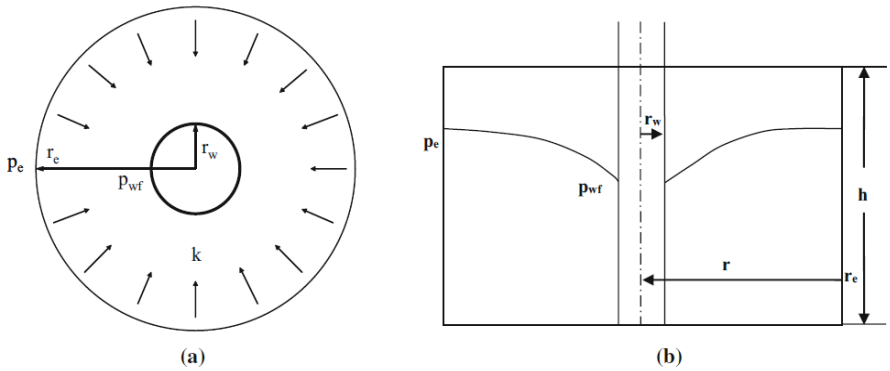

Figure 3: Flow in a circular reservoir with a well at the cenre: left – vertical view, right – lateral view.

The BL method for linear immiscible displacement was modified for radial flow by (Ling, 2016) and verified by (Zhang, 2013). Radial fractional flow is described by equation (5) while equation (6) calculates the position of a specified water saturation. These underlying assumptions of equation 2 and 3 were also applied for equation 5 and 6, that were: capillary pressure effects can be neglected, no dip and gravity forces can be neglected, homogeneous and isotropic porous medium. They enable the fractional flow evaluation of the water front position, the breakthrough time and oil recovery performance for a radial waterflooded oil reservoir.

$$fw = \frac{1+\frac{2\pi hkk_{ro}}{q_t\mu_o}\left(r\frac{\partial P_c}{\partial r}+P_c\right)}{1+\frac{k_{ro}\,\mu_w}{k_{rw}\,\mu_o}} \tag{5}$$

$$r_{Sw} = r_e - \sqrt{{r_e}^2 - \frac{WI}{\pi h\phi}\left(\frac{\partial f_w}{\partial S_w}\right)_{S_w}} \tag{6}$$

r_e is radius of the reservoir outer boundary, r_{Sw} is the position of water saturation Sw in the radial system, WI is the cumulative volume of injected water, *h* is the reservoir thickness in the radial system (see Figure 3).

2.3. Review of DP method and its extension to incorporate AWC performance

An injection and a production well are a distance L apart in a heterogeneous reservoir with non-communicating layers being waterflooded with piston-like displacement (Figure 4).

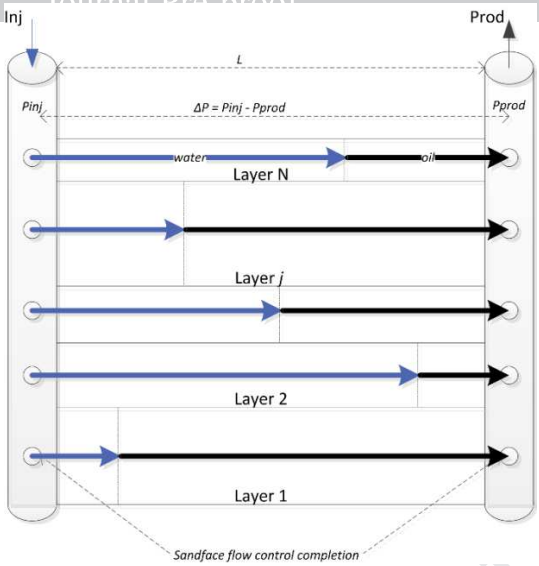

Figure 4: Oil displacement between an injection well and a production well in a heterogeneous reservoir.

Each layer has unique properties: height *h*, effective cross-sectional area *A*, porosity *φ*, horizontal permeability *k*, end point saturations S_{wi} and S_{or}. All fluid volumes and Darcy velocity (U_o and U_w) are measured at reservoir conditions.

Mobility of displacing phase: $\grave{\lambda_w} \equiv \frac{\grave{K_{rw}}}{\mu_w}$ (7)

Mobility of displaced phase: $\grave{\lambda_o} \equiv \frac{\grave{K_{ro}}}{\mu_o}$ (8)

End-point mobility ratio $M \equiv \frac{\grave{\lambda_w}}{\grave{\lambda_o}}$ (9)

$$U_o = -\frac{k\grave{\lambda_0}\Delta P_o}{L-x} \quad (10)$$

$$U_w = -\frac{k\grave{\lambda_w}\Delta P_w}{x} \quad (11)$$

Where L is the distance between injector and producer, and x is the waterfront's distance to the injector, Figure 5 shows layer *j* when the waterfront has travelled to coordinate x_j.

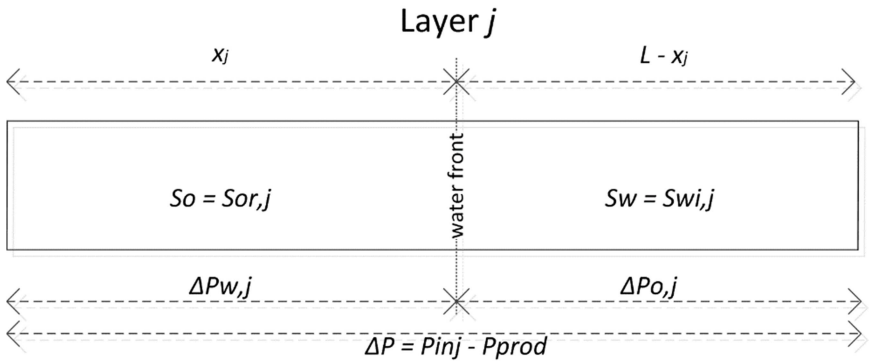

Figure 5: Saturation profile in Layer j.

All fluids are assumed to be incompressible, hence $U_o = U_w = U$. Also, $\Delta P = \Delta P_o + \Delta P_w$ allowing equation 10 and 11 to be combined to give the oil production rate (equation 12).

$$q_j = u_j A_j = \frac{k_j \grave{\lambda}_{w,j} A_j}{L} \frac{\Delta P}{x_j^* + M_j\left(1 - x_j^*\right)} \quad (12)$$

Where *x** is defined as dimensionless front distance $\grave{x}_j \equiv \frac{x_j}{L}$

(Dykstra and Parsons, 1950) provided a workflow for estimating the vertical sweep efficiency of a heterogeneous oil reservoir with non-communicating layers and piston-like fluid displacement. They provide an analytical solution for the water front position *x* in arbitrary Layer j at the exact time when the given reference Layer R is experiencing water breakthrough (i.e. when x^*_R=1 so Layer *R* is flooded). The integral solution can be expressed explicitly as:

$$x_j^* = \frac{M_j - \sqrt{M_j^2 + F_{j,R}(1 - M_j)(1 + M_R)}}{M_j - 1} \quad (13)$$

Where $F_{j,R} \equiv \frac{k_j \grave{\lambda}_{w,j}}{\Delta S_j \emptyset_j} . \frac{\Delta S_R \emptyset_R}{k_R \grave{\lambda}_{w,R}}$ and.

The movable fluid saturation, *ΔS,* defined as $\Delta S = 1 - S_{wi} - S_{or}$, allows equation 13 to be simplified to $x_j^* = \frac{F_{j,R}\,(1 + M_R)}{2}$ when $M_j = 1$.

The distance of the waterfront, and the water volume injected, in a layer after it has been flooded may be found by changing the integration limits. The water front location in the remaining layers can be calculated at the time when the first, or reference, layer experiences breakthrough. The overall reservoir saturation, the injected water volumes and the production well's fractional flow f_w (or watercut WC) can all be calculated at this time. The reservoir water saturation and the injected water volume as a function of the production well's WC is calculated by repeating the workflow as the next, and each subsequent, layer experiences water breakthrough.

(Reznik et al., 1984) and (El-Khatib, 1985) accurately included time into the model by integrating the analytical solution for x_j . We will show later that time can be approximated by matching the injection rates and the injected volumes, i.e. $t_{bt,R} \approx \left.\frac{WI_R}{q_R}\right|_{at\ x_R^* = 1}$ for AWCs by including the reservoir-to-AWC well, pressure drop system (Figure 6).

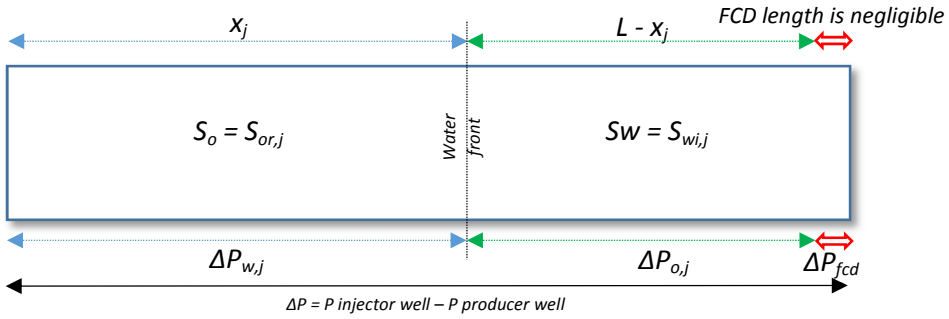

Figure 6: Calculation of fluid saturation profiles in layer j when FCDs are installed.

The pressure drop across the sandface flow control completion (ΔP_{FCC}) is a quadratic function of the flow rate where *a* is a function of the FCD strength, the number of FCDs per completion zone and the flowing fluid's properties (Al-Khelaiwi, 2013):

$$\Delta P_{FCD} = a_{flowingphase}\, q^2 \quad (14)$$

For simplicity we refer to $a_{flowingphase}$ as a_w and a_o for water and oil flow respectively. The total pressure drop across a layer is now a function of both the reservoir and the FCD:

$$\Delta P = \Delta P_{injector} + \Delta P_{layer} + \Delta P_{producer} = \left(a_{inj} + a_{prod}\right)q^2 + \Delta P_{layer} = a^* q^2 + \Delta P_{layer} \tag{15}$$

where a^* for a given layer equals $a^* \equiv a_{bbt}^* = a_{w,inj} + a_{o,prod}$ before water breaks through this layer, and $a^* \equiv a_{abt}^* = a_{w,inj} + a_{w,prod}$ after water breakthrough. Changing the *a* coefficients allows modelling of any type of FCD for any or all layers:

- A *Passive* FCD, an *Active* FCD or an *Autonomous* FCD completion: The *a* coefficients are selected to match the number and type of FCD's for each layer for either oil (producer before break through) or water (injector and producer after break through).
- a = 0 for a conventional well (no FCDs).
- $a_{w,prod} = \infty$ or $q_{abt}=0$ represents closure of the zone by a well workover, an *Active* FCD or an *Autonomous* FCD responding to a change in the flowing fluid's phase cut.

Rearranging equation (15) calculates the layer sandface-to-sandface pressure drop (ΔP_{layer}):

$$\Delta P_{layer} = \Delta P - a^* q^2 \tag{16}$$

Substituting ΔP for ΔP_{layer} in equation (12) results in $q_j = \frac{k_j \lambda_{w,j}^{`} A_j}{L} \cdot \frac{\Delta P - a_j^* q_j^2}{x_j^* + M_j(1 - x_j^*)}$ which is input into the equation *u=q/A* to yield:

$$U_j = \frac{-B_j + \sqrt{B_j^2 + 4\, a_j^* A_j^2 C_j^2 \Delta P}}{2\, a_j^* A_j^2 C_j} \tag{17}$$

where coefficients B and C are defined as:

$$B_j \equiv x_j^* + M_j\left(1 - x_j^*\right) \tag{18}$$

$$C_j \equiv \frac{k_j + \lambda_{w,j}^{`}}{L} \tag{19}$$

N.B. The original DP method includes the effective layer cross-sectional area when calculating the flow rates and watercuts. Our study of AWCs case requires the area to be introduced immediately since it affects the reservoir pressure drop. The effective cross-sectional area must be estimated, taking into account e.g. the areal sweep efficiency, flood patterns, faults, etc. (Muradov, et al., 2018) provides the complete derivation, verification and application of the DP method extended to AWCs for the piston-like fluid displacement.

3. Extending waterflood analysis with AWCs to non-piston-like displacement

3.1. Application of the Welge method for calculation of oil and water production rates

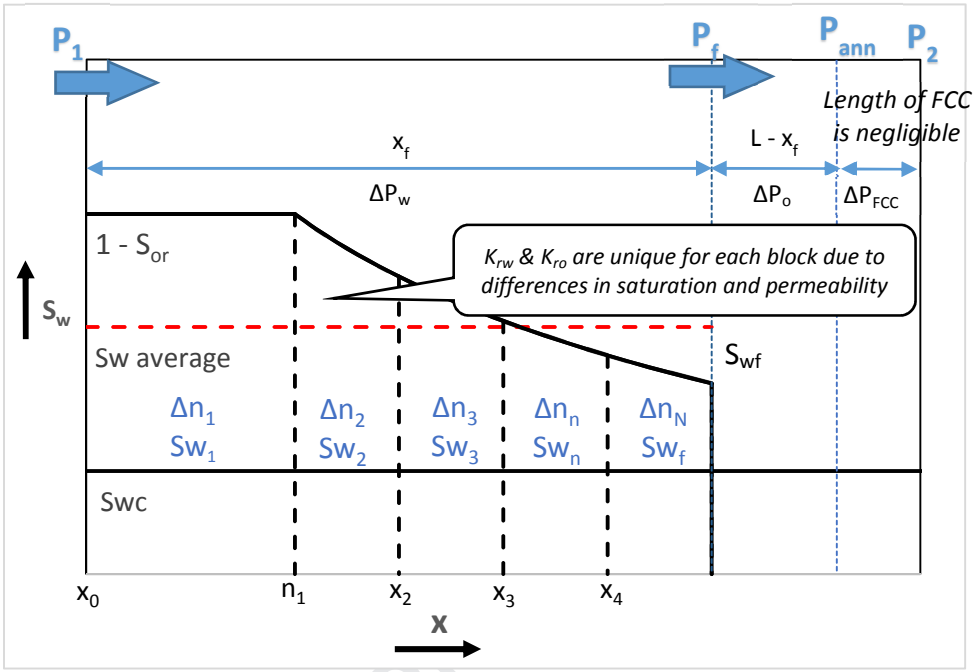

Figure 7: The formation volume behind the flood front is divided into multiple blocks

Welge analysis was developed to determine the oil recovery and the water fraction as a function of cumulative volume of water injected for non-piston-like displacement. The Welge method calculates the formation's water saturation ($\overline{S_w}$) behind the flood front assuming the oil is homogeneously displaced with water. The formation behind this flood front has a "pseudo" relative-permeability, $\overline{K_{rw}}$ & $\overline{K_{ro}}$, based on the average water saturation, $\overline{S_w}$, (Ahmed, 2001); (Craig, 1993) and (Dake, 2001) all proposed predicting the front's displacement by finding the *Kr* values by direct correlation from the value of $\overline{S_w}$ based on the actual relative-permeability curve. This assumes both piston-like displacement and linear relative-permeability curves.

Figure 7 illustrates waterflooding a layer's formation volume between the producer and the injector. P_1 refers to pressure at the injection well's location (x_0) or at the start time of the displacement process. P_f is the pressure at x_f, the tip of saturation front where water is displacing oil. The difference between pressure P_1 and P_f is ΔP_w. Mobile oil is present in the formation between the water front and the producer ($L - x_f$). ΔP_O is the pressure difference between the displacement front and the production well's annulus and $\Delta P_{FCD\ (or\ FCC)}$ is the pressure different across the FCDs. Figure 7 indicates that FCDs are only installed in the producer, an extra pressure drop, ΔP_{FCDi}, must be added to ΔP_w if FCDs are also installed in the injection well.

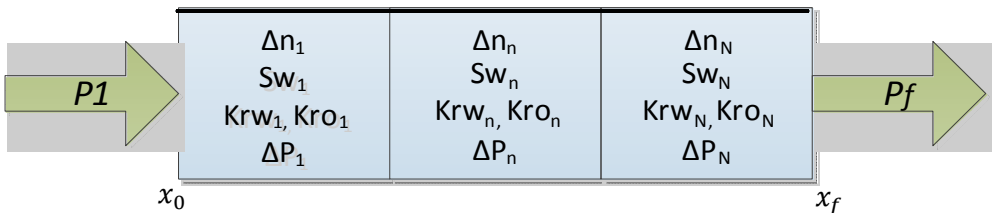

Figure 8: Several blocks with different relative permeability values are created behind the water front.

The water saturation value (Sw) of the formation between the injector and the water front gradually decreases from (1 – Sor) at the injector to Swf at waterfront (Figure 7). This can be modelled by a series of blocks with appropriate water saturation and relative permeability values (Figure 8) starting from x_0 to n_1 (= Δn_1) and continuing to block N and Δn_N (or x_f). $(P_1 - P_f)$, the pressure difference between x_0 and x_f, is equal to the sum of the pressure drops across all the blocks between x_0 and x_f (Figure 8 and equation 20).

$$P_1 - P_f = \sum_{n=1}^{N} \Delta P_n \tag{20}$$

As displayed in figure 8, the region between x_0 and x_f is consisted with unique Krw & Kro for each blocks. Our proposed method treated this region as a one block with an averaged relative permeability value for each phase, Krw_{avg} and Kro_{avg}. Thus, neglecti

ng capillary pressure:

$$Uw \frac{\mu_w X_f}{k\, krw_{avg}} = \left(Uw \frac{\mu_w (x_1 - x_0)}{k\, krw_1} + Uw \frac{\mu_w (x_2 - x_1)}{k\, krw_2} + \cdots \right) = Uw \frac{\mu_w}{k} \left(\sum_{n=1}^{N} \frac{\Delta x_n}{krw_n} \right)$$

The average oil and water relative permeability behind the water front are:

$$krw_{avg} = \frac{X_f}{\sum_{n=1}^{N} \frac{\Delta x_n}{krw_n}} = \frac{X_f}{\sum_{1-Sor}^{Swf} \frac{\Delta x_{Sw}}{Krw_{Sw}}} \tag{21}$$

$$kro_{avg} = \frac{X_f}{\sum_{n=1}^{N} \frac{\Delta x_n}{kro_n}} = \frac{X_f}{\sum_{1-Sor}^{Swf} \frac{\Delta x_{So}}{Kro_{Sw}}} \tag{22}$$

The mobility value of the displacing phase behind the flood front together with the system mobility ratio (equation 23 and 24) is now calculated:

$$\lambda_{mix,displacing\ phase} = \frac{\bar{k}_{rw}}{\mu_w} + \frac{\bar{k}_{ro}}{\mu_o} \tag{23}$$

$$Mobility\ Ratio = M = \frac{M_{Displacing}}{M_{Displaced}} = \frac{\lambda_{mix,displacing\ phase}}{\lambda_o} \tag{24}$$

The BL method determines both the position, x_n, and its saturation value, Sw_n. (Dake, 2001) explains that the position of any water saturation is proportional to the derivative of fractional flow over the water saturation (equation 25), allowing the position of each saturation block relative to the front (equation 26) to be determined.

$$X_{Sw} \propto \left. \frac{\partial f_w}{\partial S_w} \right|_{Sw} \tag{25}$$

$$\frac{X_{Swn}}{X_{Swf}} \propto \frac{\left. \frac{\partial f_w}{\partial S_w} \right|_{Swn}}{\left. \frac{\partial f_w}{\partial S_w} \right|_{Swf}} \tag{26}$$

This approach will be called the 'Extended Welge' (EW) method.

3.2. Extension of linear fractional flow analysis to include AWCs.

Fractional flow analysis integrating the extended DP, BL and EW methods, as per (Muradov, 2018)'s methodology, is possible by adding the FCD's, non-linear pressure drop to the system (equation 15). The fluid velocity in each layer is:

$$U_j = \frac{-B_j + \sqrt{B_j^2 + 4\, a_j^*\, A_j^2\, C_j^2\, \Delta P}}{2\, a_j^*\, A_j^2\, C_j} \quad (27)$$

Where coefficients B and C are:

$$B_j \equiv x_j^* + M_j\left(1 - x_j^*\right) \quad (28)$$

$$C_j \equiv \frac{k_j\, \lambda_{mix,diplacing\ phase}}{L} \quad (29)$$

Note that one of the main difference with the extended DP method's equation is the value of the mobility ratio of the displacing phase, $\lambda_{avg,diplacing\ phase}$, as explained in following section.

3.2.1 Workflow for extending linear fractional flow analysis to include AWCs.

Time period between the start of injection and water breakthrough in layer R

Step 1. Fractional flow analysis is carried out using relative permeability values to calculate, and draw, the f_w and $f_w{}'$ curves, find the value for the flood front saturation and the average water saturation (Figure 2: , equation 4 and 5). The saturation front (S_{wf}) and average water saturation($\bar{S}_w$) behind the front are constant prior to breakthrough. Kro_{avg} and Krw_{avg} of the displacing front will also be constant during this period.

Step 2. The evaluation is for every incremental x starting from the x_0 (the location of injector) to L (the location of producer). E.g. An injection and a production well are 1000 m apart and evaluated at 10 m intervals, thus x_0 represents the injection wells location, $\Delta x = 10$ m, L $= 1000$ m, and hence x_{100} is the producer's location. Note that this Δx grid is different to the N blocks in Figure 8 that represented the multiphase fluid properties. Strictly speaking, there are N blocks each time the front advances by Δx with the incremental cumulative water injection (ΔWI_k) being evaluated using equation 30 (i.e. fractional flow analysis is executed for every x_n).

$$\Delta WI_x = \frac{PV}{{df_w}/{dS_w}\big|_x} * \Delta x \quad (30)$$

Averaging the injection rate between $\mathrm{I_{x-1}}$ and $\mathrm{I_x}$ gives the incremental time (equation 31):

$$\Delta t_x = \frac{\Delta WI_x}{I_x,avg} \quad (31)$$

Equation 24 calculates the mixed fluids' mobility ratio, the injection rate is given by equations 17, 18, 19 and the total injection time by equation 32:

$$t_x = \sum_{x=1}^{X} \Delta t_x \quad (32)$$

Step 3. The above is repeated for each layer of the well's completion. *Layer R,* the reference layer, is the first layer to experience breakthrough and the remaining layers are ordered by increasing breakthrough time. The time required for the water to advance by Δx in *layer R* (equation 33) is also used to calculate the distance ($\Delta x_{j,x}$) the water advances in the other layers *(layer J)*. This distance is approximated by replacing the right side of equation 33 with equations 30 and 31.

$$\Delta t_{R,x} = \Delta t_{j,x} \tag{33}$$

$$\Delta t_{R,x} = \frac{PV_J}{df_w/_{dS_w}\big|_j} * \frac{\Delta x_{j,x}}{I_{j,x,avg}} \tag{34}$$

The first two parameters $\left(\frac{\mathrm{PV_J}}{\mathrm{df_w}/_{\mathrm{dS_w}}\big|_{\mathrm{j}}}\right)$ on the right-hand side of equation 34 are constant before breakthrough at Swf_j, hence only Δx needs be calculated. The injection rate (I) is also a function of Δx, a simple non-linear solver (e.g. Excel, Matlab) can determine this in a fraction of second.

Step 4. Repeat step 3 until *layer R* experiences breakthrough. Flow-in and flow-out of the system are equal (i.e. $Q_o = I$) during this time period. No water is produced and $Q_w = 0$.

Time period after initial water breakthrough until all completion layers are producing water.

Step 5. The second layer to experience breakthrough is now designated as *layer R* and steps 3 and 4 are repeated until water breaks through into all remaining layers. The post-water breakthrough into those layers experiencing water breakthrough (*layer K*) is calculated by evaluating every incremental S_w starting from the initial flood front saturation, Swf_k, until when oil production stops, i.e. $S_w = (1 - S_{OR})$. E.g., *layer K* experiences an initial water front saturation of 0.45 and has a residual oil saturation of 0.2. The oil and water production rates are calculated by equation 35, 36 and $I_K = (Q_o + Q_w)_K$. This is repeated in increments of $\Delta S_w = 0.05$ from $Sw_{k,1} = 0.45$ to $Sw_{k,8} = 0.80$, after which *Layer K* produces 100% water.

$$Q_o = \frac{I}{f_w} - I \tag{35}$$

$$Q_w = I - Q_o \tag{36}$$

Equations 37 provides the time required to increase ΔS_w by 0.05 in *layer R.* This time is also used to calculate the increase in water saturation in the other layers (*layer K*).

$$\Delta t_{R,x} = \Delta t_{k,s} \tag{37}$$

Layer K's increase in the water saturation ($\Delta S_{k,s}$) is approximated by replacing the right hand side of equation 37 with equations 30 and 31.

$$\Delta t_{R,x} = \frac{1}{df_w/_{dS_w}\big|_{k,s} * I_{k,s,avg}} * PV_R \tag{38}$$

Water has already broken through in *layer K*. Hence, equation 38 it is now necessary to determine the first two parameters on the right-hand-side of equation 38, $\frac{1}{\mathrm{df_w}/_{\mathrm{dS_w}}\big|_{\mathrm{s}}(\mathrm{I_{k,s,avg}})}$, both of which are function of S_w. A non-linear solver is required to solve for the value for $Sw_{k,s}$ also provides the change in the mixed fluid's mobility ratio (equation 29) and the injection rate (equations 17, 18 and 19).

Step 5a. An extra calculation step is required to evaluate the (variable) "strength" parameter (a^*_{abt}) when *autonomous* FCDs are installed This is obtained from equation 39 (Halvorsen, Elseth and Nævdal, 2012; Mathiesen, Werswick and Aakre, 2014).

$$a_{ICD}{}^{*}_{abt} = \left[\frac{[(WC*\rho_w)*((1-WC)*\rho_o)]^2}{\rho_{cal}}\right] \cdot \left[\frac{\mu_{cal}}{[(WC*\mu_w)*((1-WC)*\mu_o)]}\right]^{y} \cdot a_{AICD} \quad (39)$$

Steps 5 and 5a are repeated until all layers are producing water.

Time period after all layers have experienced water breakthrough.

Step 6. All layers are designated *layer k* apart from *layer R,* the last layer to experience breakthrough. The step 5 workflow continues is repeated until the well's oil production ceases and $S_w = (1 - S_{OR})$ in all layers (equation 40).

$$\Delta t_{R,x} = \Delta t_{k,s}$$

$$\frac{1}{{df_w}/{dS_w}\big|_{R,s} * I_{R,s,avg}} * PV_R = \frac{1}{{df_w}/{dS_w}\big|_{k,s}(I_{k,s,avg})} * PV_k \quad (40)$$

Step 7. Summing each layer's performance: cumulative oil produced, N_p (equation 41), cumulative water produced, W_p (equation 42), cumulative water injected, W_{inj} (equation 43) at any time.

$$N_p = \sum_{t=0}^{n} Q_{oil}|_t \cdot \Delta t \quad (41)$$

$$W_p = \sum_{t=0}^{n} Q_{water}|_t \cdot \Delta t \quad (42)$$

$$W_{inj} = \sum_{t=0}^{n} Q_{inj}\big|_t \cdot \Delta t \quad (43)$$

3.2.2. Extending the workflow for constant well production

The workflow for constant rate well production requires approximating the layer rates prior to the breakthrough at an arbitrary pressure drop by calculating the flow rates at every x (equations 27, 28 and 29). Their sum gives the total well rate. The pressure drop required for the chosen well rate is found as previously with an optimisation routine. This process is repeated for each Δx prior to breakthrough after which it is repeated for each ΔS_w increment.

3.3. Radial fractional flow analysis extended to an AWC.

The total layer pressure drop from the reservoir boundary to the well (equations 44 and 45) is the sum of the pressure drops across the: (1) displacing phase from the external reservoir radius, r_e, to the flood front, r_f, (2) displaced phase from the flood front, r_f, to the wellbore radius, r_w, and (3) flow through the flow control completion:

$$\Delta P = \Delta P_{Displacing} + \Delta P_{Displaced} + \Delta P_{FCC} \quad (44)$$

$$\Delta P = \frac{q\, ln\left(\frac{r_e}{r_f}\right)}{h\, k\, \lambda_{mix}} + \frac{q\, ln\left(\frac{r_f}{r_w}\right)}{h\, k\, \lambda_o} + a^* q^2 \quad (45)$$

Rearranging equation 45 gives:

$$Q_j = \frac{-B_j + \sqrt{B_j^2 + 4\, a_j^* \left(P_e - P_{wf}\right)}}{2\, a_j^*} \quad (46)$$

Where:

$$B_j \equiv \frac{\frac{1}{M}ln\left(\frac{r_e}{r_f}\right)+ln\left(\frac{r_f}{r_w}\right)}{h\ k\ \lambda_o} \quad (47)$$

The section 3.1. workflow for linear displacement is followed to obtain λ_{mix} by discretising the displacing phase into N blocks to find the average oil and water relative permeability values for radial flow (equations 48 and 49):

$$krw_{avg} = \frac{ln\left(\frac{r_e}{r_e - r_f}\right)}{\sum_n^N\left(\frac{ln\left(\frac{r_e - n_{(n-1)}}{r_e - n_{(n)}}\right)}{krw_n}\right)} \quad (48)$$

$$kro_{avg} = \frac{ln\left(\frac{r_e}{r_e - r_f}\right)}{\sum_n^N\left(\frac{ln\left(\frac{r_e - n_{(n-1)}}{r_e - n_{(n)}}\right)}{kro_n}\right)} \quad (49)$$

The water front's advance in radial displacement is no longer directly proportional to the derivative of fractional flow. The radial case requires the position ($n_{(n)}$) for each saturation block (Sw_n) to be solved with equation 50, a modified version of equation 6. Fractional flow analysis assumes incompressible fluids and volume replacement, hence the cumulative water injected (WI) equals the cumulative liquid produced (V).

$$V_n = \frac{PV}{df_w/_{dS_w}\big|_n} * \sum_{n=1}^{n} \Delta n_n$$

$$n = r_e - \sqrt{{r_e}^2 - \frac{V_n}{\pi h \phi}\left(\frac{\partial f_w}{\partial S_w}\right)_{S_{wn}}} \quad (50)$$

AWC cases with radial flow replace the *Δx* employed for linear displacement with *Δr*.

4. Verification of the waterflood, analytical model.

4.1. A single layer, linear waterflood

A single layer, box, reservoir model with a cross sectional area of 30 m^2 and 500 m spacing between the production and the injection wells was constructed in the ECLIPSE™ numerical reservoir simulator for validation of our analytical, waterflood performance workflow. The 50 bar pressure difference between the two wells and the oil/water mobility ratio of 5 ensured linear, non-pistonlike, oil displacement. Table 1 summarises the other reservoir properties. The production well's *autonomous* FCD completion had a pre-breakthrough strength (a^*_{bbt}) of 0.008 bar/(rcm/d)^2 which gradually increased to 0.064 bar/(rcm/d)^2 at 100% WC.

Table 1 - Well adata for the linear flow, waterflood validation test

Parameters	K	W	h	ϕ	S_{wi}	S_{or}	k_{we}	k_{oe}	μ_w	μ_o	n_o	n_w	a^*_{bbt}	a^*_{abt}	ΔP
Units	*mD*	*m*	*m*						*cP*	*cP*			$\frac{bar}{(rcm/day)^w}$		*bar*
Value	4000	10	3	0.4	0.2	0.15	0.5	0.95	0.4	4	2	3	0.008	0.064	50

$$k_{ro} = k_{roe}\left(\frac{(S_o - S_{or})}{(1 - S_{wc} - S_{or})}\right)^{n_o} \quad (51)$$

$$k_{rw} = k_{rwe}\left(\frac{(S_w - S_{wc})}{(1 - S_{wc} - S_{or})}\right)^{n_w} \quad (52)$$

(Brooks-Corey, 1966)'s relative permeability curves (equations 51 and 52) allow explicit calculation of the f_w and $f_w{}'$ values (equations 53 and 54). n_o and n_w, are the Brooks-Corey exponents for oil and water and k_{roe} and k_{rwe} are the relative permeability curve end points.

$$f_w = \frac{1}{\left(1 + \frac{\frac{\mu_w}{\mu_o}\frac{k_{roe}}{k_{rwe}}(S_o - S_{or})^{n_o}\cdot(1 - S_{wc} - S_{or})^{n_w}}{(S_w - S_{wc})^{n_w}(1 - S_{wc} - S_{or})^{n_o}}\right)} \quad (53)$$

$$f_w{}' = \frac{df_w}{dS_w} = (f_w - f_w^2)\left(\frac{n_o}{(1 - S_w - S_{or})} + \frac{n_w}{(S_w - S_{wc})}\right) \quad (54)$$

Figure 9 finds the water saturation at the flood front (Sw_f = 0.575), and the average saturation behind the front (Sw_{avg} = 0.65). The calculation is repeated at 50 m intervals between injector's (x_0) the producer's (x_{10}) location. The discretised harmonic average (HA) method with 50 blocks behind the front, (i.e. N=50), for calculating the average relative-permeability (equations 21 and 22) and estimating Q_{inj} and Q_o for each block better reproduced the ECLIPSE™ results than the Welge method (Figure 10 and Table 2). This mismatch increased further after water breakthrough (Figure 10).

Table 2: Comparison of the average relative permeability prior to water breakthrough

Average relative permeability prior to water breakthrough		
	Kro-avg	**Krw- avg**
Harmonic Average	**0.01**	**0.15**
Welge	**0.13**	**0.13**

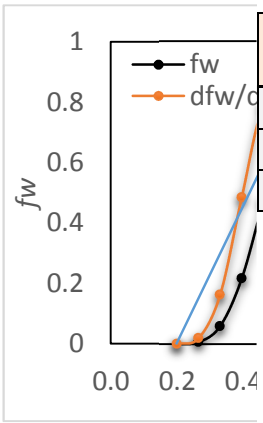

Figure 9: Numerical and analytical comparison of fractional flow analysis for a linear waterflood

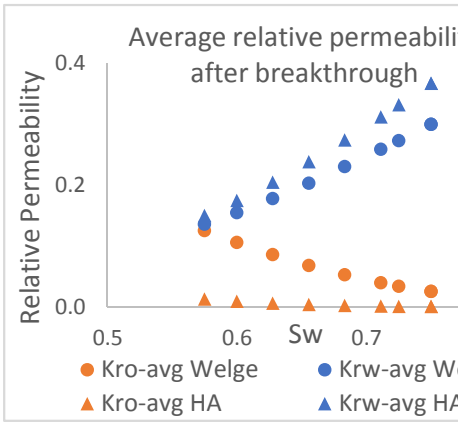

Figure 10: The harmonic average and Welge methods compared

Our analytical model's water and oil production rates agree well with the results of numerical simulation (Figures 11 and 12).

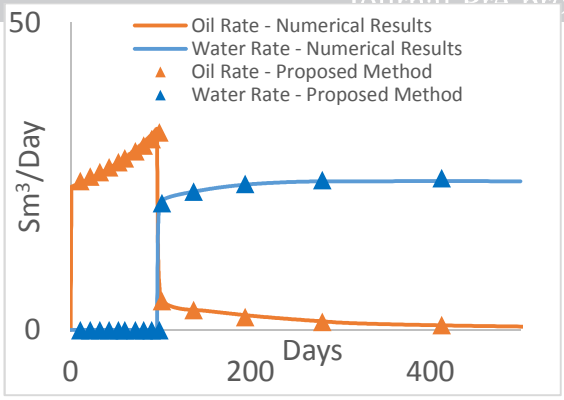

Figure 11: Water and Oil production rates

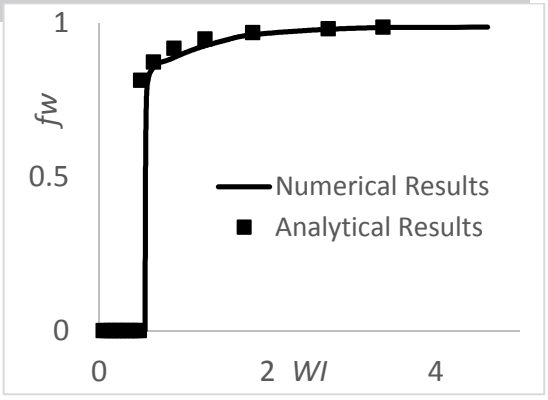

Figure 12: Water Injection (WI) versus water-cut (fw)

4.2. A single layer, radial waterflood

The reservoir radius (r_e) is 91.4 m, the thickness (h) 1.52 m and the permeability is 0.2 Darcy. The production well, 0.03 m diameter, is completed with *autonomous* FCDs of strength (a^*_{bbt}) 0.011 bar/(rcm/d)^2 prior to breakthrough, increasing gradually to 0.043 bar/(rcm/d)^2 at 100% WC. Voidage replacement and a constant ΔP was maintained between the wells. Fluid properties are as per section 4.1. Table 3 summarises the well and reservoir data.

Table 3 - Well and reservoir data for the radial flow, waterflood validation test.

Parameter	K	r_e	r_w	h	ϕ	S_{wi}	S_{or}	k_{we}	k_{oe}	μ_w	μ_o	n_o	n_w	a^*_{bbt}	a^*_{abt}	ΔP
Units	*Darcy*	*m*	*m*	*m*						*cP*	*cP*			*bar/(rcm/d)2*		*bar*
Value	0.2	91.4	0.03	1.52	0.2	0.2	0.10	0.5	0.95	0.4	4	2	3	0.011	0.043	289

The linear-flood workflow was followed with the average permeability being calculated by the Welge and HA methods. The same fluids properties were used, giving the same saturation values at the flood front and the average saturation behind the front (Sw_f = 0.57 and Sw_{avg} = 0.65). However, the HA relative permeability values in radial flow are different (Figures 13 and 14) since they are calculated at positions (X_j) that depend on a logarithmic calculation of the front's position.

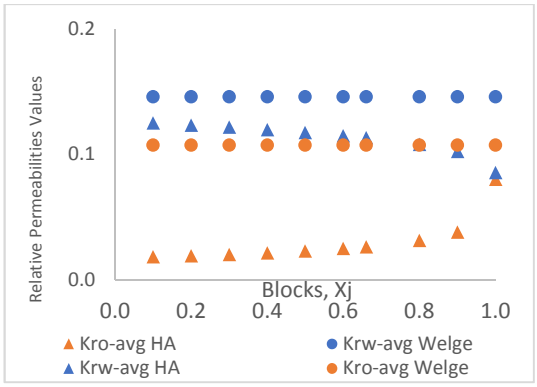

Figure 13: Average relative permeability calculation methods before breakthrough for a radial flood

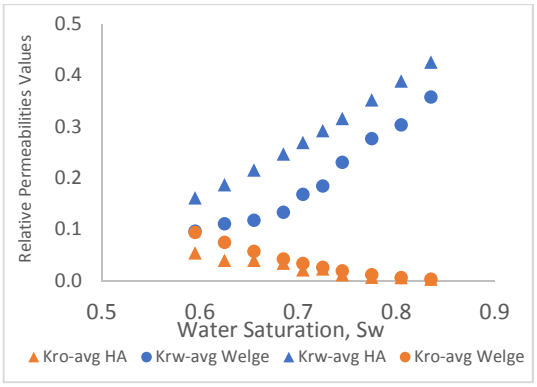

Figure 14: Average relative permeability calculation methods after breakthrough

The fluid production rates before and after breakthrough (Figure 15) and the fractional flow evaluation (Figure 16) validate our analytical methods against the Eclipse™ reservoir simulator.

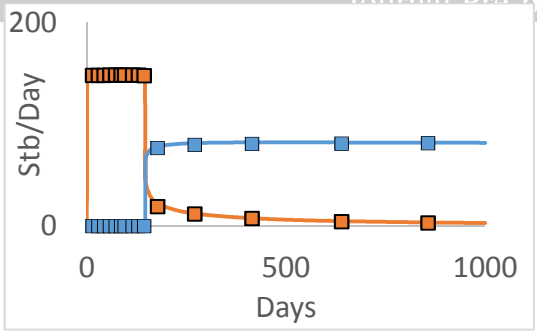

Figure 15: Numerical (line) and analytical (squares) results for water (blue) and oil (red) production rates compared for a radial waterflood.

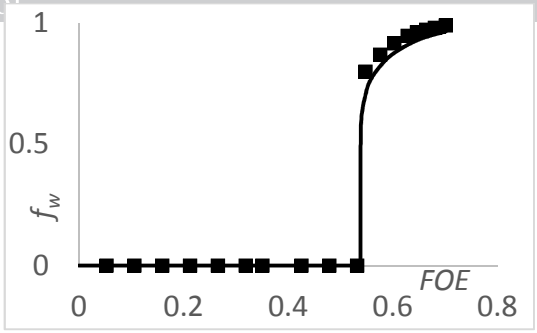

Figure 16: Comparison of numerical (line) and analytical (squares) results for Field Oil Recovery (FOE) versus water-cut (f_w) for a radial waterflood.

4.3. Verification for the multi-layer linear, non-piston like displacement case

A non-communicating, multilayer, box-shaped reservoir model with the same properties (Table 4) as that used in (Muradov, et al, 2018). Relative permeabilities were described by a (Brooks-Corey, 1966) function. The water (μ_w) and oil (μ_o) viscosities are 0.4 cP and 4 cP respectively. An injection and a production well were placed at opposite ends of the box's long axis. The production well's *autonomous* FCD completion has strength of 0.008 bar/(rcm/d)^2 when producing 100% oil, increasing gradually to 0.064 bar/(rcm/d)^2 for 100% water production. The FCD's strength increases by a factor of 8, a value sufficient to delay excessive water production while still allowing an economic level of oil production once the water front has arrived at the production well. Layer voidage replacement maintained a constant 50 bar pressure difference between the flowing bottom-hole injection and production pressures. Steps 1 to 7 (section 3.2.1) tracks the position of the water front in each layer as it progresses between the wells.

Table 4 - Properties of the linear waterflooding in a multi-layer reservoir completed with AWC.

Parameters	K	h	φ	μ_w	μ_o	S_{wi}	S_{or}	k_{we}	k_{oe}	Area	n_o	n_w
Units	mD	m		cP	cP					m^2		
1 (top)	5000	5	0.45	1	4	0.2	0.1	0.5	0.95	50	2	3
2	1000	7	0.25	1	4	0.2	0.25	0.4	1	70	2	3
3	300	9	0.2	1	4	0.2	0.4	0.6	1	90	2	3
4	2000	6	0.3	1	4	0.2	0.3	0.7	1	60	2	3
5	4000	3	0.4	1	4	0.2	0.15	0.5	1	30	2	3

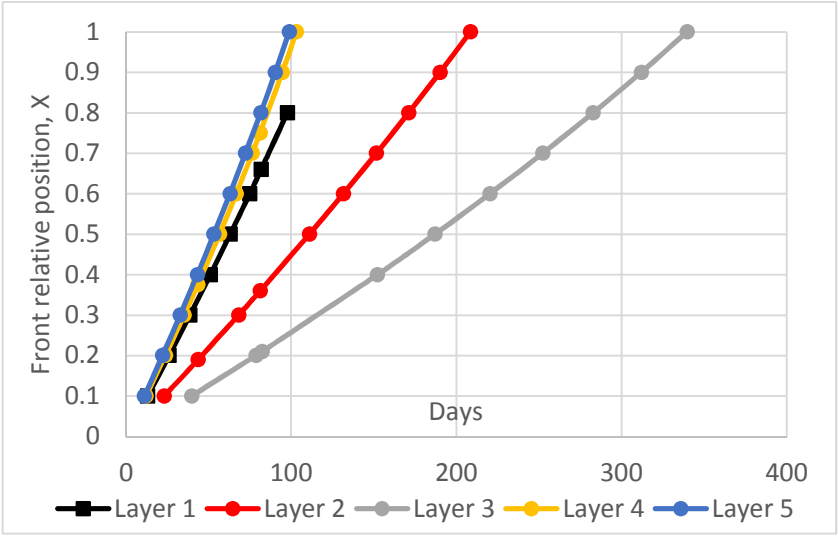

Figure 17: The layer front position vs time for each layer calculated with our analytical model.

Figure 18 and Figure 19 are snapshots of the numerically simulated, water saturation at x_R = 0.4 and x_R = 0.8 for the bottom, highest permeability, reference layer where the initial water breakthrough occurs. The improved sweep efficiency of the *autonomous* FCD completion compared to screen completion is illustrated in Figures 20 and 21, water saturation snapshots for the screen completion at the same time step as Figures 18 and 19.

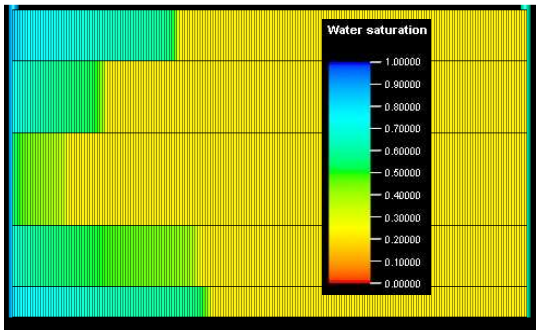

Figure 18: Layer water saturation at X_R = 0.4 for the autonomous *FCD completion*

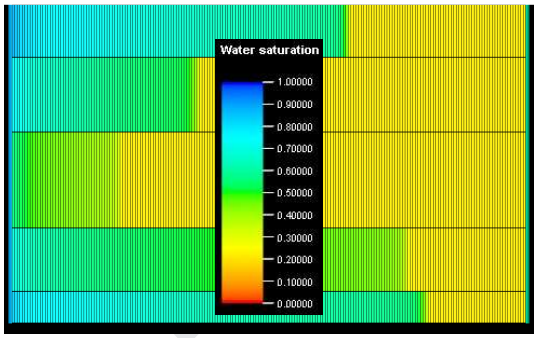

Figure 19: Layer water saturation at X_R = 0.8 for the autonomous *FCD completion*

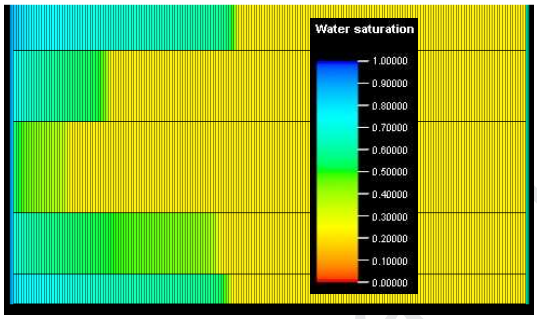

Figure 20: Layer water saturation profile for the screen completion at the time step as Figure 18.

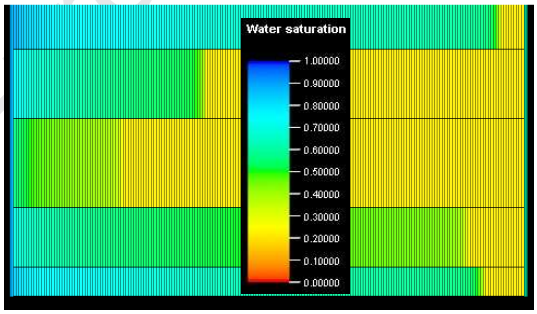

Figure 21: Layer water saturation profile for the screen completion at the time step as Figure 19.

The workflow calculates a different value of the injection rate Q_{inj} for each X_n in order to maintain voidage replacement along with the position of the water front in the time domain (Figure 22). The average, layer K_{rw}, K_{ro} values change such that the injection rate in layer 5 increases during the first 100 days prior to break after which its flow is restricted by the FCD. The process is repeated as each subsequent layer experiences breakthrough, resulting in the layer flow rates being relatively more equal as the flood continues.

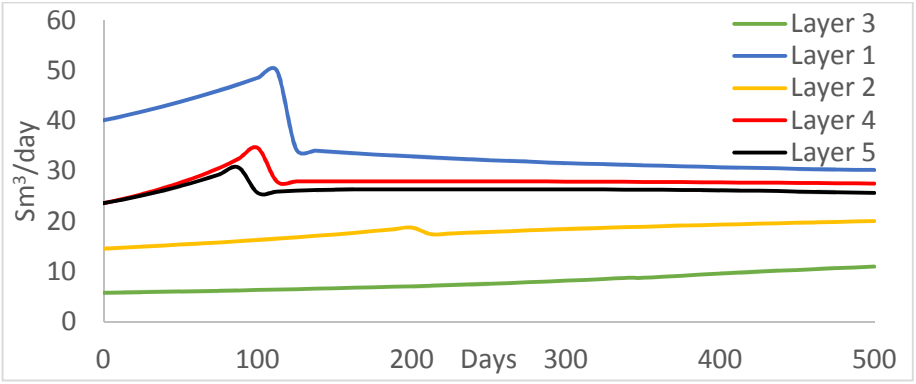

Figure 22: Predicted layer flow rates over time

The good agreement between the numerical (lines) and analytical results (squares) for the well oil (red) and water (blue) flow rates and the cumulative production is displayed in Figures 23 and 24.

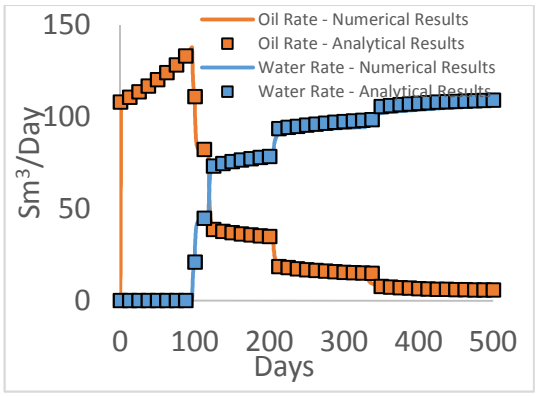

Figure 23: Comparison of numerical and analytical prediction of oil and water production rates

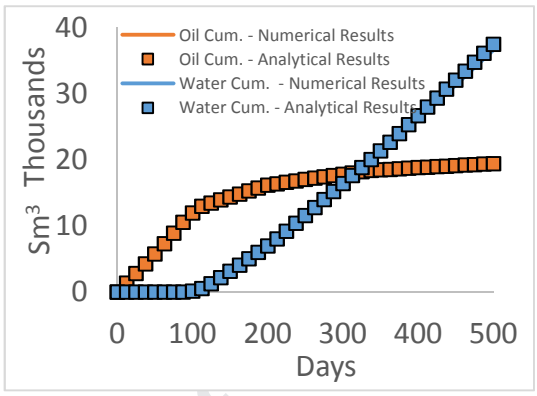

Figure 24: Comparison of numerical and analytical prediction of oil and water cumulative production

4.4. Selection of an optimised AWC

We have shown how our method transforms the waterflood performance into the time domain. This allows economic analysis of the many possible options for well completion design to be performed rapidly, such as for the multi-layer reservoir described in Table 4. The Net-Present-Value (NPV), a common economic analysis tool, will be used to choose the optimum *autonomous* FCD completion design drawn from (Table 5), the available hardware options.

$$NPV = \sum_{k=1}^{M} \Delta t \, \frac{Q_o r_o + Q_w r_w - Q_l r_{opex}}{\left(1+{}^{b}/_{100}\right)^{t_k}} \qquad (55)$$

Where M is the total number of time steps. Δt is the difference between two time steps in days. Q_o, Q_w, Q_l is respectively oil, water, and liquid production rate in bbl/d. r_o is oil price in USD/bbl, r_w is the cost of water operation in USD/bbl, r_{opex} is the operation cost in USD/bbl, b is in the discount rate percent per year, and t_k is the elapsed time in years.

We employ our method to calculate the oil and water production rates (Figure 25 and Figure 26) that are converted to monthly revenue and cost values, allowing the a^*_{bbt} *and* a^*_{abt}values that give the highest NPV to be identified based on the Table 5 economic data.

Evaluation of all these scenarios using reservoir simulation would require considerable time and computing resources, as illustrated by (Eltaher *et al.*, 2014). Our method replaces the numerical reservoir simulation, at least for the rough optimisation of the vertical sweep.

Table 5 - AFCD completion scenarios

	a^*_{bbt}	a^*_{abt}	remarks
Scenario number	**bar/(rcm/d)²**	**bar/(rcm/d)²**	
1	0	0	Screen
2	0	0.008	AFCD
3	0	0.016	AFCD

4	0	0.064	AFCD
5	0.008	0	AFCD
6	0.008	0.008	ICD
7	0.008	0.016	AFCD
8	0.008	0.064	AFCD
9	0.016	0	AFCD
10	0.016	0.008	AFCD
11	0.016	0.016	ICD
12	0.016	0.064	AFCD
13	0.064	0	AFCD
14	0.064	0.008	AFCD
15	0.064	0.016	AFCD
16	0.064	0.064	ICD

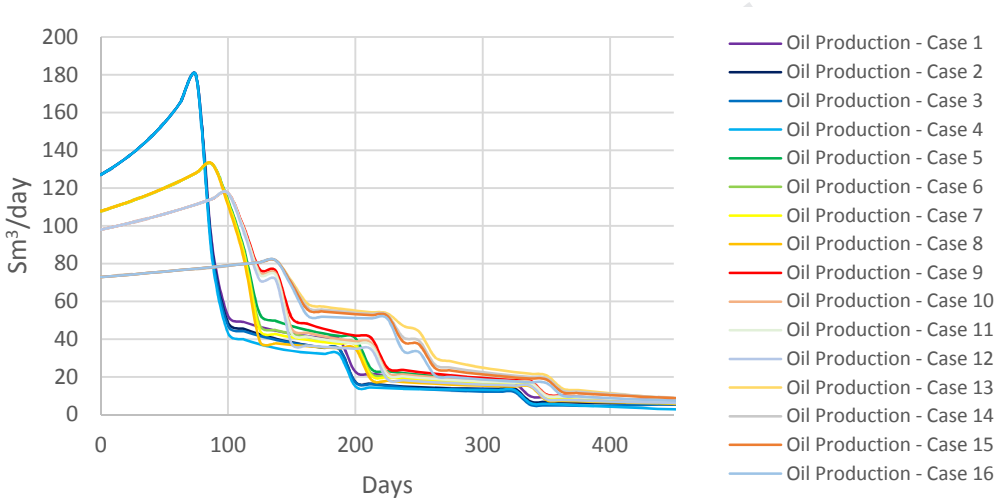

Figure 25: Comparison of oil production for scenario 1 - 16

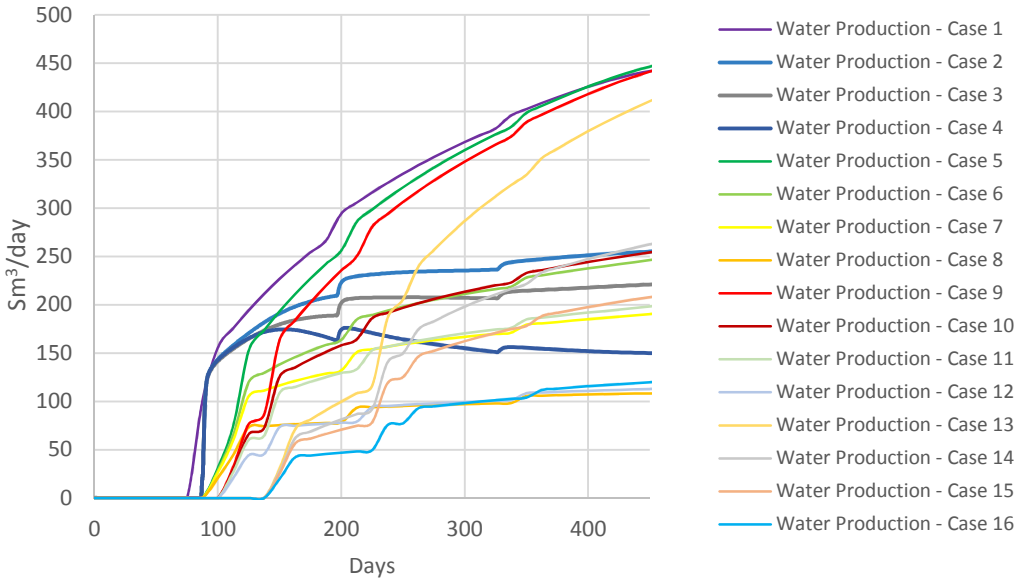

Figure 26: Comparison of oil production for scenario 1 – 16

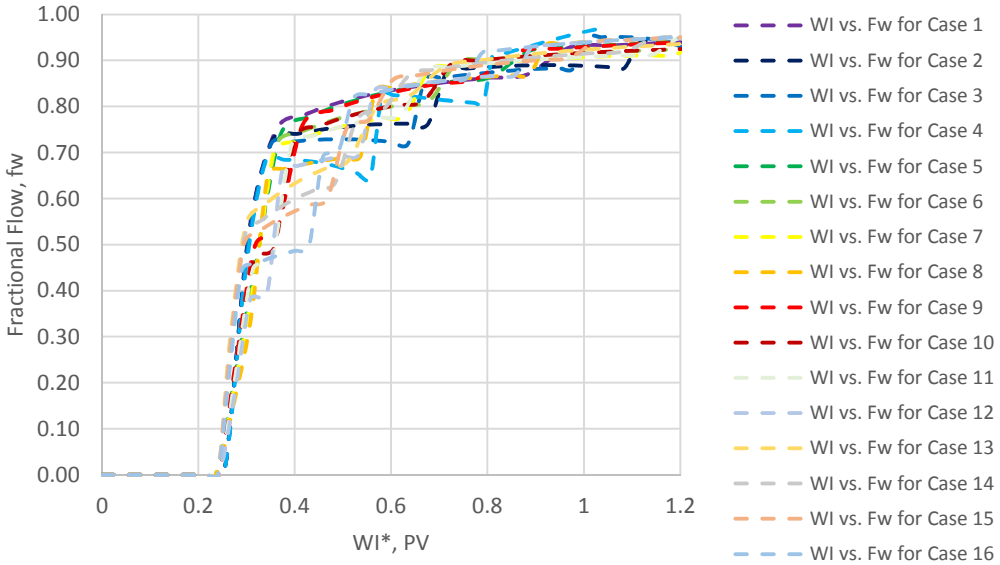

Figure 27: Comparison of Fw vs. WI results for scenario 1 - 16*

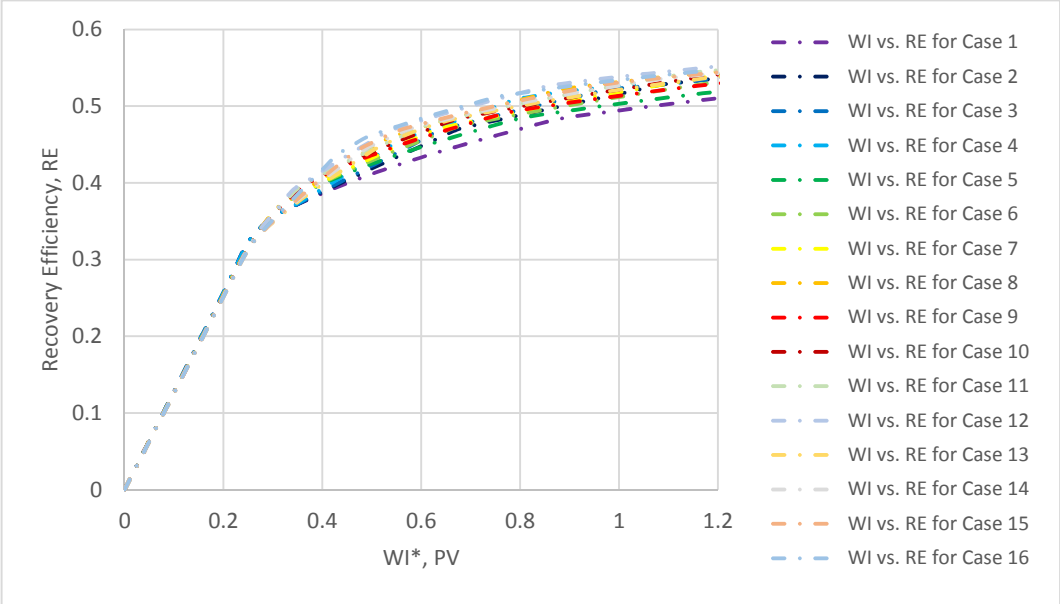

Figure 28: Comparison of RE vs. WI results for scenarios 1 - 16*

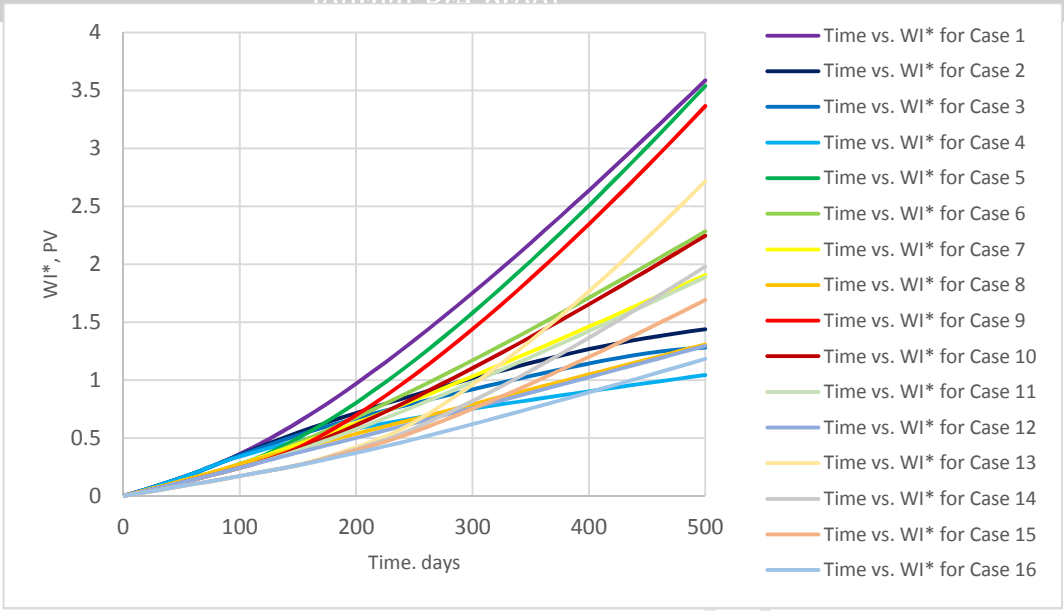

Figure 29: Comparison of WI vs. time results for scenarios 1 - 16*

The workflow can also compare the fractional flow (f_w) and recovery efficiency (RE) as a function of the injected water volume (WI*). Figure 27, Figure 28 and Figure 29 provide a long-term (500 day) analysis of the FCDs' performance in terms of the field cumulative oil (Figure 30) and water (Figure 31) production.

Our method provides greater insight into the well's performance than the frequently used "snapshot" optimisation (Halliburton, 2017). At a minimum it provides an initial optimisation of the completion's vertical sweep efficiency. It can remove the need for numerical analysis in many reservoir scenarios, though further study may be required in some cases.

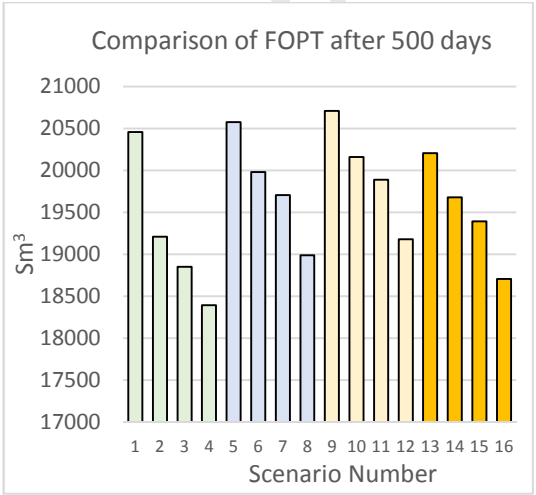

Figure 30: Scenario 1 - 16 FOPT

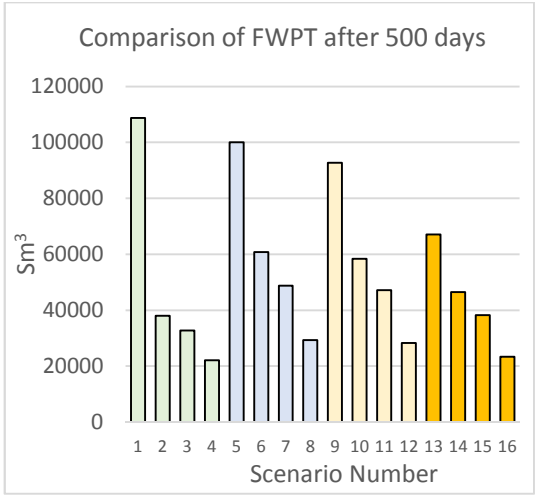

Figure 31: Scenario 1 – 16 FWPT

Increasing the FCD strength before breakthrough (a^*_{bbt}) initially increases the FOPT (Figure 30, scenarios 1, 5 and 9). This trend reverses once the restriction becomes excessive given the 50 bar pressure difference between the injection and production wells. Increasing a^*_{bbt} also reduces the FWPT (Figure 31, scenarios 1, 5 and 9), a result that may improve outflow performance in some well designs. Prakasa et al. (2015) and Prakasa et al. (2019) noted a similar trade-off between well productivity and flow equalisation.

Comparing Figure 30 and 31 scenarios with the same colour shows a significantly reduced water and oil production when the FCC strength is increased after breakthrough (a^*_{abt}). This observation is reversed for "piston-like displacement (M < 1). Here an increasing a^*_{abt} reduces FWPT with little effect on FOPT (Eltaher, 2017).

The general trends in Figure 30 and Figure 31 are similar, with the higher a^*_{bbt} strengths reducing FWPT water faster than FOPT. This behaviour will not always occur, increasing a^*_{bbt} for fluids with a high mobility ratio (M >>1) reduces FOPT more than FWPT (Eltaher, 2017).

The figure 30 and 31 production data can be further analysed to provide the figure 32 "quick look" project economic predictions with the Table 6 economic data.

The scenarios with the highest FOPT (1, 5, 9, and 13), i.e. those with a low FCC strength before breakthrough (a^*_{bbt}), do not provide the best economic results. However, installing an FCD to minimise FWPT, i.e. scenario 16 with an aggressive a^*_{bbt} and a^*_{abt}, reduces both the FOPT and the NPV.

Scenarios 2, 6, 10, and 14 are completed with the same a^*_{abt}, but perform differently. Each of these scenarios has a different recovery before breakthrough and hence a different added-value due to the time dependence of money. Each scenario has different water front dynamics and will exhibit different control by a given post-breakthrough flow restriction. The effect of a^*_{abt} thus depends on the restriction before breakthrough (a^*_{bbt}).

Table 6 - Assumptions for economic calculation

Oil Price	Water Handling Cost	Operational Cost	CAPEX	Discount factor	Discount factor
$/m3	**$/m3**	**$/m3**	**$/10^{3}m^3**	**%/Year**	**%/month**
314.47	6.29	9.43	0.00	15.00	1.17
$/stb	**$/stb**	**$/stb**	**$/10^{3}stb**		
50	1.00	1.50	0		

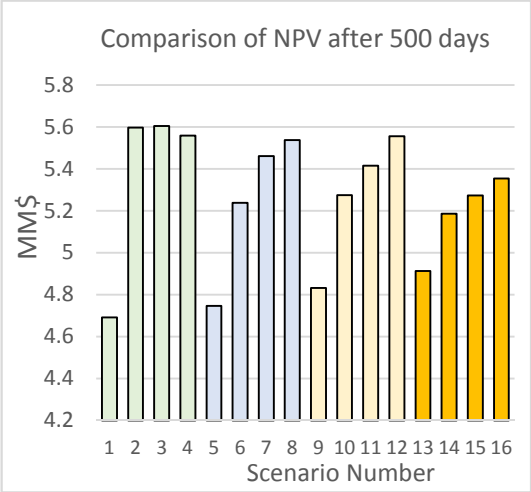

Figure 32: Scenario 1 – 16: NPV

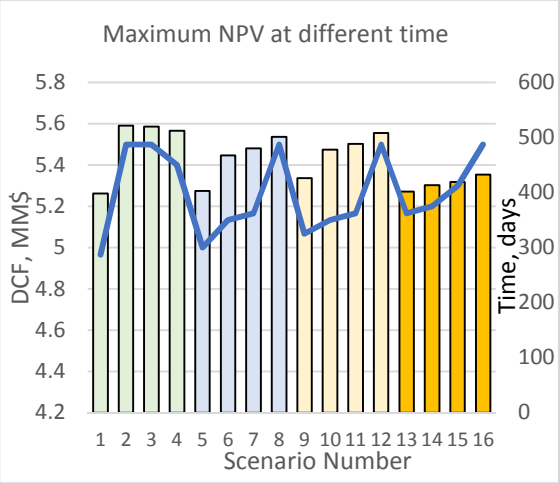

Figure 33: Scenario 1-16: Time of maximum NPV

The best results are also not a design that is fully open to oil and very restrictive to water. The optimum scenario (2, 3, 8 and 12) have an optimized restriction for oil and an optimized restriction for water for the most economically attractive project. The "optimum" strength completion design depends on both the early-time and the later-time production.

Another completion evaluation criterion is the time at which the maximum NPV occurs (Figure 33). The production vs. time curves have different shape and their time of maximum

NPV differs. A declining late-time NPV (*Figure* Figure 34) indicates the project has a negative cash flow, despite still recovering oil.

Project evaluation criteria that stipulate a faster return on investment favour completions that are less aggressive to water. Scenarios 1, 5, 9 and 13 accelerate production (including water) with an early maximum NPV.

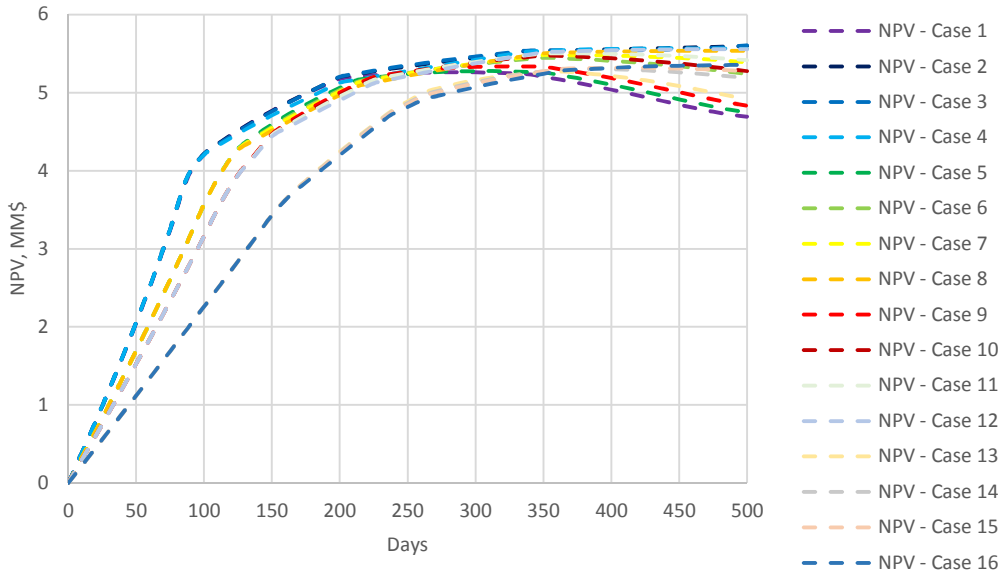

Figure 34: Comparison of NPV over time for scenario 1-16

5. Discussion and conclusion

This paper extends the classical, fractional flow analysis workflow to situations when the reservoir is developed with a waterflood exhibiting non piston-like oil displacement and the wells have been completed with downhole flow control. Our model allows fast and accurate prediction of the waterflood performance in both linear and radial cases without the need for numerical reservoir modelling. The waterflood's performance is translated into the time domain using a simple search algorithm. Solving the combined reservoir-well system in time also allows economic evaluation of the waterflooded reservoir when its performance is influenced by the control provided by the well completion.

The optimum downhole flow control completion is determined by the water cut dynamics. *Autonomous* FCDs, the latest development in downhole flow control completions, change the strength of their flow restriction as a function of the water cut. This work's prediction of the water cut using fractional flow analysis for such completions means that their fluid production and economic performance can be analysed without resorting to numerical reservoir simulation.

It is known that the optimum AFCD completion design for a reservoir exhibiting piston-like displacement is to install an AFCD with a low restriction during oil production and a reasonably aggressive restriction once water production starts. This is not the case if the reservoir exhibits non-pistonlike displacement, though there is still an optimum restriction, confirming (Eltaher, 2014)'s concept of excessive and acceptable levels of water production when designing an AFCD.

Our workflow both models and predicts the long-term value-added by FCDs. It is the bridge between simple, "snapshot" inflow evaluation and comprehensive, numerical reservoir simulation. The main objective is to provide an insight into underlying physics in the reservoir in an easily understood form, by enabling quick-look screening of completion designs with a tool that can be easily realised by most engineers employing available spreadsheet resources.

This workflow can also be used to compare the numerical simulation as a means of validation, pre-cursor, complementary tools to enhance the robustness of reservoir modelling alone.

Incorporating a description of the AWC's performance into the waterflood analysis model allows forecasting the down flow control configuration's production profile, the oil recovery and the economic gain. Our method is particularly useful for rapidly designing and optimising a completion that maximizes a chosen criterion, e.g. oil recovery, economic value-added, etc. The complexity of existing modelling tools ensures that this task is rarely examined in detail.

The reservoir sweep models forming the basis of these tools have been thoroughly verified. They provide a simplified, fast, analysis of the impact of various well completion and control options on the development and efficiency of a waterflood. The method's transparency and ease of implementation of its algorithms can make it a useful tool for well and reservoir engineers.

6. Nomenclature

All values are in SI units and at reservoir conditions, unless otherwise stated.

A - effective area perpendicular to flow	a - flow control completion strength defined by equation 14
b - formation volume factor	f_w - fraction flow rate of water (watercut at downhole conditions)
h - layer height	k - horizontal permeability
L - distance between wells	M - mobility ratio
n - exponent for modified Brooks-Corey functions	ΔP - pressure difference
P - pressure	P_c – Capillary pressure
q - flow rate	re - The external reservoir radius (the peripheral oil-water contact)
rf - The radius distance of the flood's front	rw - wellbore radius
S - saturation	ΔS - movable saturation ($1-S_{or}-S_{wi}$)
t - time	u - fluid flow velocity
V - Cumulative liquid produced	x - The distance index for front advancement evaluation between injector and producer
λ - fluid mobility (i.e. rel.perm./viscosity)	$\frac{df_w}{dS_w}$ = Fractional flow derivative

Subscripts

abt - after breakthrough	avg - average
ann - annulus	bt - breakthrough
bbt - before breakthrough	e - external
f – denote the saturation or the location of flood front	Fcc – flow control completion
Injector – pressure drop occur at injector well	j, k, R - referes to Layer j, k, or R respectively
Layer – pressure drop occur at layer	N - Number of blocks with different water saturations behind the flood front
n - the block's index (behind the front) for average relative permeability calculation	o - oil
oh - Openhole	or - residual oil (saturation)
Producer – pressure drop occur at producer well	r - relative (permeability)
s - The saturation index for postwater	w - water

breakthrough evaluation	
wi - irreducible water (saturation)	wf - waterfront

Superscripts

a^* - total FCC flow restriction coefficient for a layer, defined as $a^*=a_{producer}+a_{injector}$
WI* - volume of water injected expressed in reservoir pore volumes
x* - relative water front position defined as x* = x/L
λ' - end-point mobility
fw' – derivative of fractional flow over water saturation

Abbreviations

AICD	Autonomous Inflow Control Device (a class of FCDs)
AFCD	Autonomous Flow Control Device (a class of FCDs)
AWC	Advanced Well Completion
BL	Buckley-Leverett
DP	Dykstra-Parsons
DCF	Discounted Cash Flow
EW	Extended Welge
FCC	Flow Control Completion (equivalent with FCD)
FCD	Flow Control Device
FOE	Field Oil Recovery
FOPT	Field Oil Production Total (Cumulative oil production)
FWPT	Field Water Production Total (Cumulative water production)
HA	Harmonic Average
NPV	Net Present Value
PV	(reservoir) pore volume
Rcm	(at) Reservoir conditions - cubic meters (units)
RE	Oil Recovery Efficiency (recovery factor)
WI	Volume of Water Injected

7. Acknowledgement

The authors thank the sponsor of the Value from Advanced Wells (VAWE) Joint-Industry project at Heriot-Watt University for the support. The authors also thank Schlumberger Information Solutions for the access to their software.

8. References

Ahmed, T. 2001, Reservoir Engineering Handbook (Second addition), Gulf Professional Pub. ISBN: 0884157709, 9780884157700.

Al-Khelaiwi, Faisal T, Vasily M Birchenko, Michael R. Konopczynski et al. 2008. Advanced Wells: A Comprehensive Approach to the Selection between Passive and Active Inflow Control Completions. Presented at the International Petroleum Technology Conference, Kuala Lumpur, Malaysia. IPTC- 12145-MS. https://doi.org/10.2523/IPTC-12145-MS

Al-Khelaiwi, 2013, A Comprehensive Approach to the Design of Advanced Well Completions. PhD Thesis. Heriot-Watt University.

Birchenko, V. M., A. Iu Bejan, A. V. Usnich et al. 2011. Application of inflow control devices to heterogeneous reservoirs (in Journal of Petroleum Science and Engineering 78 (2): 534-541. http://dx.doi.org/10.1016/j.petrol.2011.06.022.

Brooks, R.H. and Corey, A.T., 1966. Properties of porous media affecting fluid flow. Journal of the Irrigation and Drainage Division, 92(2), pp.61-90.

Buckley, S. E., & Leverett, M. C. (1942, December 1). Mechanism of Fluid Displacement in Sands. Society of Petroleum Engineers. doi:10.2118/942107-G

Craig, F. F., Jr.1993, The Reservoir Engineering Aspects of Waterflooding, Monograph Series, Richardson, Texas, SPE, (1993), 3.

Dake, L. 2001. The Practice of Reservoir Engineering (Revised Edition), Volume 36, ISBN: 9780080574431

Deppe, John C. 1961. Injection Rates - The Effect of Mobility Ratio, Area Swept, and Pattern. SPE J 1 (02). https://doi.org/10.2118/1472-G

Dyes, A. B., B. H. Caudle, R. A. Erickson. 1954. Oil Production After Breakthrough as Influenced by Mobility Ratio, SPE-309-G, http://dx.doi.org/10.2118/309-g.

Dykstra, H. and Parsons, R.L., 1950. The prediction of oil recovery by water flood. Secondary recovery of oil in the United States, 2, pp.160-174.

El-Khatib, Noaman. 1985. The Effect of Crossflow on Waterflooding of Stratified Reservoirs (includes associated papers 14490 and 14692 and 15043 and 15191). SPE J 25 (02). SPE 11495-pa. http://dx.doi.org/10.2118/11495-pa.

El-Khatib, Noaman. 1999. Waterflooding Performance of Communicating Stratified Reservoirs With Log-Normal Permeability Distribution. SPE Res Eval & Eng 2 (06). SPE-59071-pa. http://dx.doi.org/10.2118/59071-pa.

El-Khatib, Noaman A. 2012. Waterflooding Performance in Inclined Communicating Stratified Reservoirs., Presented at the SPE North Africa Technical Conference and Exhibition, 14-17 February, Cairo, Egypt. SPE-126344-ms. http://dx.doi.org/10.2118/126344-ms.

El-Khatib, Noaman A. F. 2003. Effect of Gravity on Waterflooding Performance of Stratified Reservoirs. Presented at the SPE Middle East Oil Show, 9-12 June, Bahrain. SPE-81465-ms, http://dx.doi.org/10.2118/81465-ms.

Eltaher, Eltazy Mohammed Khalid, Morteza Haghighat Sefat, Khafiz Muradov et al. 2014. Performance of Autonomous Inflow Control Completion in Heavy Oil Reservoirs. Presented at the International Petroleum Technology Conference, 10-12 December, Kuala Lumpur, Malaysia. IPTC-17977-ms. https://doi.org/10.2523/IPTC-17977-MS

Eltazy Eltaher, Khafiz Muradov, David Davies, Peter Grassick, 2018. Autonomous flow control device modelling and completion optimisation, Journal of Petroleum Science and Engineering. https://doi.org/10.1016/j.petrol.2018.07.042

Goddin, C. S., Jr., F. F. Craig, Jr., J. O. Wilkes et al. 1966. A Numerical Study of Waterflood Performance In a Stratified System With Crossflow. JPT 18 (06). SPE-1223-pa, http://dx.doi.org/10.2118/1223-pa.

Haghighat Sefat, Morteza, Khafiz M. Muradov, Ahmed H. Elsheikh et al. 2016. Proactive Optimization of Intelligent-Well Production Using Stochastic Gradient-Based Algorithms. SPE Res Eval & Eng 19(02). SPE-178918-pa. http://dx.doi.org/10.2118/178918-pa.

Halliburton (2017), NETool List of publications. Halliburton

Henriksen, Knut Herman, Eli Iren Gule, Jody R. Augustine. 2006. Case Study: The Application of Inflow Control Devices in the Troll Field. Presented at the SPE Europec/EAGE Annual Conference and Exhibition, 12-15 June, Vienna, Austria. SPE-100308-MS. http://dx.doi.org/10.2118/100308-ms.

Hiatt, W.N., 1958, January. Injected-fluid coverage of multi-well reservoirs with permeability stratification. In Drilling and Production Practice. American Petroleum Institute.

Johnson, Carl E., Jr. 1956. Prediction of Oil Recovery by Waterflood - A Simplified Graphical Treatment of the Dykstra-Parsons Method. JPT 8 (11). SPE-733-G. http://dx.doi.org/10.2118/733-g.

Johnson, J. P. 1965. Predicting Waterflood Performance by the Graphical Representation of Porosity and Permeability Distribution. SPE. doi:10.2118/918-PA

Ling, Kegang. 2012. Fractional Flow in Radial Flow System - A Study for Peripheral Waterflood. Presented at the SPE Latin America and Caribbean Petroleum Engineering Conference, 16-18 April, Mexico City, Mexico. SPE-152129-MS. https://doi.org/10.2118/152129-MS

Ling, Kegang, 2016. Fractional flow in radial flow systems: a study for peripheral waterflood. Journal of Petroleum Exploration and Production Technology 6 (03). https://doi.org/10.1007/s13202-015-0197-3

Livescu, S., Brown, W. P., Jain, R., Grubert, M., Ghai, S. S., Lee, L.-B. W., & Long, T. 2010. Application of a coupled wellbore/reservoir simulator to well performance optimization. Presented at the SPE Annual Technical Conference and Exhibition, Florence, Italy. SPE-135035-MS. https://doi.org/10.2118/135035-MS

Mijic, A., and T. C. LaForce (2012), Spatially varying fractional flow in radial CO2-brine displacement,Water Resour. Res., 48, W09503, doi:10.1029/2011WR010961.

Muradov, K. M., Prakasa, B., & Davies, D. (2018, August 1). Extension of Dykstra-Parsons Model of Stratified-Reservoir Waterflood To Include Advanced Well Completions. Society of Petroleum Engineers. doi:10.2118/189977-PA

Muradov, K, Eltaher, E & Davies, DR 2018, 'Reservoir simulator-friendly model of fluid-selective, downhole flow control completion performance' Journal of Petroleum Science and Engineering, vol. 164, pp. 140-154. DOI: 10.1016/j.petrol.2018.01.039

Muscat, M. 1950. The effect of permeability stratification in complete water-drive systems (in Trans., AIME: 349-358.)

Osman, Mohammed E., Djebbar Tiab. 1981. Waterflooding Performance and Pressure Analysis Of Heterogeneous Reservoirs. Presented at the SPE Middle East Technical Conference and Exhibition, 9-12 March, Bahrain. SPE-9656-MS. http://dx.doi.org/10.2118/9656-ms.

Prakasa, B., Muradov, K., & Davies, D. (2015, September 8). Rapid Design of an Inflow Control Device Completion in Heterogeneous Clastic Reservoirs Using Type Curves. Society of Petroleum Engineers. doi:10.2118/175448-MS

Prakasa, B, Muradov, K & Davies, DR 2019, 'Principles of rapid design of an Inflow Control Device Completion in Homogeneous and Heterogeneous Reservoirs Using Type Curves' Journal of Petroleum Science and Engineering, vol. 176, pp. 862-879. DOI: 10.1016/j.petrol.2019.01.104

Reznik, A. A., Robert M. Enick, Sudhir B. Panvelker. 1984. An Analytical Extension of the Dykstra-Parsons Vertical Stratification Discrete Solution to a Continuous, Real-Time Basis (includes associated papers 13753 and 13830 and 14873 and 14695). SPE J 24 (06). http://dx.doi.org/10.2118/12065-pa.

Rossen, W.R., Johns, R.T., Kibodeaux, K.R., Lai, H. and Tehrani, N.M., 2008, September. Fractional-flow theory applied to non-Newtonian IOR processes. In ECMOR XI-11th European Conference on the Mathematics of Oil Recovery.

Snyder, R. W., H. J. Ramey, Jr. 1967. Application of Buckley-Leverett Displacement Theory to Non-communicating Layered Systems, JPT 19 (11). http://dx.doi.org/10.2118/1645-pa.

Warren, J. E. 1964. Prediction of Waterflood Behavior in a Stratified System. SPE J 4 (02). http://dx.doi.org/10.2118/581-pa.

Welge, H., “A Simplified Method for Computing Oil Recovery by Gas or Water Drive,” Trans. AIME, 1952, pp. 91–98.

Williams, G. J. J., Mansfield, M., MacDonald, D. G., & Bush, M. D. 2004. Top-Down Reservoir Modelling. Presented at the SPE Annual Technical Conference and Exhibition, Houston, U.S.A. SPE-89974-MS. https://doi.org/10.2118/89974-MS.

Wu, Y.-S., Fakcharoenphol, P., & Zhang, R. (2010, January 1). Non-Darcy Displacement in Linear Composite and Radial Flow Porous Media. Society of Petroleum Engineers. doi:10.2118/130343-MS

Zhang, H., Ling, K., & Acura, H. (2013, April 15). New Analytical Equations of Recovery Factor for Radial Flow Systems. Society of Petroleum Engineers. doi:10.2118/164766-MS

Linear and radial flow modelling of a waterflooded, stratified, non-communicating reservoir developed with downhole, flow control completions

Highlight

This manuscript presents a new approach to model reservoirs with Advanced Well Completion (AWC) that enables fast design of AWC and complements the operators' existing workflows. The fluid flow through the reservoir-AWC-well system is characterised as a much simpler proxy model (reduced-physics model), that is still comprehensive enough to capture the main characteristic of the reservoir system. It provides a simple model, that is appropriate to the available data, while hence allowing a quick scoping of concepts and options prior, or in addition, to detailed reservoir modelling. Such workflows meet the oil and gas business's preferences for simpler and faster processes.

A simple, portable toolbox is coded to determine the optimal completion response in various field/fluid conditions within the short time that is available when making a decision. Furthermore, the proposed proxy models could be enrolled as a fast initiation (or quick scoping) prior, or in addition, to detailed modelling enabling a faster work cycle.

We aims to develop a framework that enables to design ICD and AFCD completion for long-term optimisation, i.e. in the 'dynamic' reservoir flow condition. The chapter starts by providing the advantage of having a long-term strategy/outlook when designing the flow control completion. The feasibility of AWC is mainly influenced by the economic parameters, which can only be obtained once we have an outlook on the long-term results from installing the AWC. The developed model is constructed from the combination of classical waterflood displacement equations with a recently developed analytical model of a flow control completion. The idea is then extended for light-oil displacement, which replicates piston-like displacement (an extension of Dykstra-Parsons solution to AWC wells) and medium/heavy-oil displacement, which replicate non-piston like displacement (an extension of Buckley-Leverett & Welge solution to AWC wells). The model was successfully tested and verified using numerical reservoir simulation.